Frequency- and time-domain investigation of the dynamic properties of interlayer-exchange-coupled $Ni_{81}Fe_{19}/Ru/Ni_{81}Fe_{19}$ thin films

M. Belmeguenai, T. Martin, G. Woltersdorf, M. Maier, and G. Bayreuther
Institut für Experimentelle und Angewandte Physik, Universität Regensburg, Universitätsstraße 31, 93040 Regensburg, Germany
(Received 24 February 2007; revised manuscript received 25 May 2007; published 14 September 2007)

Pulsed inductive microwave magnetometer (PIMM), conventional ferromagnetic resonance (FMR), and vector network analyzer FMR (VNA-FMR) have been used for complementary studies of the various excited modes in exchange-coupled NiFe(30 nm)/Ru(d_{Ru})/NiFe(30 nm) films with variable Ru thicknesses d_{Ru}. For antiferromagnetically coupled layers, two modes, which vary in their relative intensity as a function of the bias field, are detected. These two modes, which are observable simultaneously over a limited range of the bias field with PIMM, are identified as optic and acoustic modes. The mode frequencies and the interlayer exchange coupling are found to oscillate as a function of the Ru layer thickness with a period of 8.5 Å. The frequency oscillations of the optic mode are coupling dependent, while those of the acoustic mode are indirectly related to coupling via the canting angle of the layer magnetizations below the saturation. Comparison between PIMM and VNA-FMR in terms of frequency of modes shows good agreement, but the optic mode is observed over a wider field range with VNA-FMR. Furthermore, we clearly observed different behaviors of the FMR linewidths as a function of the spacer thickness for the optic and acoustic modes. In addition, perpendicular standing spin waves have been studied as a function of coupling. The FMR linewidth of the different modes increases with the microwave frequency and typical damping constants of $\alpha=0.0073$ have been measured. The effect of the pulse field amplitudes on the properties of the various excited modes has been simulated and studied experimentally.

DOI: 10.1103/PhysRevB.76.104414 PACS number(s): 75.40.Gb, 76.50.+g, 75.70.−i, 75.30.Et

I. INTRODUCTION

Exchange interlayer coupling between the magnetizations $\mathbf{M}_1$ and $\mathbf{M}_2$ of two ferromagnetic layers separated by a nonmagnetic spacer layer was demonstrated experimentally in 1986.[1–3] This coupling is parametrized by the bilinear J_1 and biquadratic J_2 coupling parameters defined via the phenomenological energy density expression:

$$E = -J_1 \frac{\mathbf{M}_1 \cdot \mathbf{M}_2}{M_1 M_2} - J_2 \left(\frac{\mathbf{M}_1 \cdot \mathbf{M}_2}{M_1 M_2} \right)^2 . \quad (1)$$

The nature and the strength of the coupling are described by the sign and the magnitude of J_1 and J_2. When J_1 dominates, and if it is positive, the energy is minimal when $\mathbf{M}_1$ and $\mathbf{M}_2$ are parallel [ferromagnetic (FM) coupling], while if it is negative, then the lowest energy is achieved when $\mathbf{M}_1$ and $\mathbf{M}_2$ are antiparallel [antiferromagnetic (AF) coupling]. If, on the other hand, J_2 dominates and is negative, then the minimum energy occurs when the magnetizations are oriented perpendicularly to each other (90°-type coupling).[4]

Later discoveries in such coupled structures including giant magnetoresistance[5,6] led to an explosion in the interest on these systems. Therefore, they are on the base of the development of many components which are considered now as potential candidates for magnetic recording devices and toggled magnetic random access memories.[7] However, the precessional dynamics at 1–10 GHz, which determines the high-speed response, is a fundamental limit to increasing data rates in magnetic information storage technology.[8] Therefore, understanding the nature, the extent of exchange interactions, and their effect on the damping in such structures at the nanosecond time scale is a technological key for such applications.

Great attention has been given in recent years to study both experimentally and theoretically the effect of coupling on spin waves in these layered systems.[9,10] Brillouin light scattering[11] and ferromagnetic resonance[12] are usually used to determine the coupling constants and to study the spin-wave modes, but only methods using pulsed excitation can reach the switching regime. At high excitation amplitudes, the motion of the magnetization becomes enharmonic, and it is best modeled by solving the Landau-Lifshitz-Gilbert (LLG) equation numerically. In addition, a FMR experiment is generally limited to a single frequency and high static magnetic fields are used, so that the amount of information obtained from a FMR measurement is rather limited and it is difficult to study the dynamics at low fields below the saturation. Therefore the aim of this paper is to use pulsed inductive microwave magnetometer (PIMM) and vector network analyzer FMR (VNA-FMR), besides a conventional FMR, for full and complementary study of the dynamics of interlayer-exchange-coupled systems both in time and frequency domain over large static and pulse field ranges. Moreover, and in contrast to the conventional FMR, VNA-FMR and PIMM allow dynamic measurements over a large frequency range. We focused our study particularly on low applied bias fields not sufficient to saturate the specimens, so that the magnetization was antiparallel or canted at a certain angle with respect to the applied field. In such situation, we show that not only the frequency of the optic mode depends on the interlayer exchange coupling but also that of the acoustic mode.

This paper is organized as follows: we first define our macrospin model and explain how the static and dynamic simulations are carried out (Sec. II). Section III introduces the samples and the different experimental setups used for

this study. Section IV starts by summarizing the main static characteristics of the samples and then presents dynamic measurements, the excited mode properties, and the comparison between time- and frequency-domain methods. This section ends by presenting the effect of the coupling on the linewidth of the different excited spin waves. The effect of the pulse field amplitudes on the properties of the excited spin-waves is studied in Sec. V, and comparison to macrospin simulation is presented. In Sec. VI, conclusions are drawn.

II. MACROSPIN CALCULATIONS

We consider two magnetic thin films, 1 and 2, of thicknesses d_1 and d_2 separated by a nonmagnetic spacer layer with thickness d. We study only the situation where the external static magnetic field **H** is applied in the plane of the films, at an arbitrary angle θ_H with respect to the easy axis direction. In this case, the directions of the magnetizations of the two films, M_1 and M_2, also in the plane, are characterized by the angles ψ_1 and ψ_2 with respect to the easy axis direction. The equilibrium directions of M_1 and M_2 are determined by the minima of the total free energy per unit area given by

$$E_{tot}(\psi_1,\psi_2) = E_{1,a}(\psi_1)d_1 + E_{2,a}(\psi_2)d_2 + E_{ex}(\psi_1,\psi_2). \quad (2)$$

The volume energy density E_a, composed of the Zeeman and anisotropy energies, and the exchange energy density E_{ex} are given by

$$E_a(\psi) = K_u \sin^2 \psi - \mu_0 M_s H \cos(\theta_H - \psi), \quad (3)$$

$$E_{ex}(\psi_1,\psi_2) = -J_1 \cos(\psi_1 - \psi_2) - J_2 \cos^2(\psi_1 - \psi_2), \quad (4)$$

where M_s is the magnetization at saturation and K_u is the uniaxial anisotropy constant.

The equilibrium configuration ($\psi_{1,equ}$ and $\psi_{2,equ}$) are determined numerically for each applied field, taking J_1 and J_2 as parameters, and the normalized static hysteresis loops are given by

$$\frac{M(H)}{M_s} = \frac{M_1 \cos(\psi_{1,eq} - \theta_H) + M_2 \cos(\psi_{2,eq} - \theta_H)}{M_1 + M_2}. \quad (5)$$

The spatiotemporal evolution of magnetization of the film i is given by the numerical solution of the equation of motion written as[13]

$$\frac{d\mathbf{m}_i(t)}{dt} = -\frac{\mu_0|\gamma|}{1+\alpha^2}\mathbf{m}_i(t) \times H_{eff,i} - \frac{\alpha\mu_0|\gamma|}{1+\alpha^2}\{\mathbf{m}_i(t) \times [\mathbf{m}_i(t) \times H_{eff,i}]\}, \quad (6)$$

where γ is the gyromagnetic ratio, α is the phenomenological damping parameter, and $H_{eff,i}$ is the effective field vector acting on the layer i with a normalized magnetization vector $\mathbf{m}_i$.

The effective field comprises the applied field **H**, the anisotropy field H_{ani}, the demagnetizing field H_{demag}, the pulse field H_{pulse}, and the bilinear and biquadratic exchange fields H_{J_1} and H_{J_2}. These exchange fields are given by

$$H_{J_1,i} = \frac{J_1}{\mu_0 M_s d_i}\mathbf{m}_j(t)$$

and

$$H_{J_2,i} = \frac{2J_2}{\mu_0 M_s d_i}\begin{pmatrix} m_{i,x}m_{j,x}^2 + m_{j,x}(m_{i,y}m_{j,y} + m_{i,z}m_{j,z}) \\ m_{i,y}m_{j,y}^2 + m_{j,y}(m_{i,x}m_{j,x} + m_{i,z}m_{j,z}) \\ m_{i,z}m_{j,z}^2 + m_{j,z}(m_{i,y}m_{j,y} + m_{i,x}m_{j,x}) \end{pmatrix}$$

with $i \neq j$. (7)

For the simulations and in order to be as close as possible to the real case, the real pulse field shape (as measured) is used. Equation (6) is numerically integrated using the initial equilibrium state obtained from the static simulation, a step size of 1 ps, and a damping parameter α=0.017 which is in a good agreement with the measured one using PIMM. Moreover, all the static and dynamic simulations which will be presented below considered the case of symmetrical magnetic layers having the same thicknesses and magnetic characteristics.

III. SAMPLES AND EXPERIMENTAL METHODS

A series of $Ni_{81}Fe_{19}/Ru(d_{Ru})/Ni_{81}Fe_{19}$ trilayered samples with a fixed $Ni_{81}Fe_{19}$ thickness of 300 Å and variable Ru thicknesses (1.6 Å$<d_{Ru}<$28 Å) was sequentially deposited at room temperature by dc magnetron sputtering onto silicon substrates with Ta seed and cover layers in a commercial sputtering system at IPHT Jena. The Ru thickness gradient (1.6–28 Å) is spread over two 6 in. wafers, on which the thickness changes from 1.6 to 9 Å and from 6 to 28 Å, respectively. The base pressure of the sputtering system was typically 10^{-8} mbar. The deposition rates were about a fraction of an angstrom per second. During the growth of the $Ni_{81}Fe_{19}$ layers, a magnetic field of 100 Oe was applied, which induced a uniaxial magnetic anisotropy with defined easy axis. The easy axes are parallel for both NiFe layers.

Magneto-optical Kerr effect (MOKE) and vibrating sample magnetometer (VSM) were used at room temperature to obtain the hysteresis loops for each sample, both in easy and hard axis directions. The measured hysteresis loops were then fitted numerically by minimizing the total energy of the system to determine the coupling constants J_1 and J_2, as described in Sec. II. For samples with FM coupling where the determination of the interlayer exchange coupling constants cannot be performed using static methods, FMR measurements have been used to determine the total coupling (effective coupling: J_{eff}). The maximum saturation fields both in easy and hard axes are in the range of 0.8–1.4 kOe for 4.6 Å$<d_{Ru}<$6.4 Å and they vary from 3 to 500 Oe otherwise.

The dynamic measurements were carried out by FMR, PIMM, and VNA-FMR. For PIMM and VNA-FMR, the samples of 1 cm^2 are coupled to a coplanar waveguide and the experimental setups are described in Refs. 14 and 15, respectively. For both methods, the data at each bias field

require the subtraction of two measurements: one with the bias field switched on and a second measurement with a 1 kOe saturating field applied in the same direction as the pulse or the rf field, which removes all magnetic response from the measured quantity (transmission coefficient: S_{21} in decibel in the case of VNA-FMR and in voltage in PIMM). By subtracting this saturated measurement from the bias field measurement, all that remains is the effect of the oscillatory response created by the precessing magnetization in the sample. In our case, a maximal bias field of 1 kOe was applied before each bias field measurement in order to define an initial state. This field was reduced to the target bias field before the voltage pulse or rf field. The resonance frequencies are obtained from the Fourier transform of the time-domain magnetic response or from the Lorentzian fit of the S_{21} measured by VNA.

For the FMR measurements, the experimental setup is the same as described in Ref. 15. The magnetic sample is mounted inside a shorted waveguide. The microwave absorption is measured by monitoring the power reflected from the sample using a mixer. The sample is swept through the resonance condition by means of an external field. When the magnetic sample undergoes a ferromagnetic resonance, the microwave losses are increased and the reflected power changes slightly. In addition, the external magnetic field is modulated with an amplitude of 2 Oe at a frequency of 130 Hz. This modulation allows lock-in detection to be used in order to increase the signal-to-noise ratio. The measured FMR signal is proportional to the field derivative of the imaginary part of the rf susceptibility. The FMR experiments were carried out using 22 and 35 GHz systems.

IV. RESULTS AND DISCUSSION

A. Static characterization

VSM hysteresis loops for a NiFe/Ru/NiFe trilayer with a 4.9-Å-thick Ru layer are shown in Fig. 1(a). The data correspond to the field aligned along the easy and hard axes. The hysteresis loop in the hard axis has been shifted horizontally by 100 Oe for clarity. Comparison of the two curves indicates that the anisotropies in the system are small. Note the slow approach to saturation above 0.5 kOe for both cases. This asymptotic behavior, regardless of field orientation, suggests that a strong coupling exists across the Ru film. The remanence is large, between 55% and 60% of saturation depending on field orientation. It is possible to explain the remanence and approach to saturation with the presence of a large biquadratic coupling between the ferromagnetic layers across the Ru spacer. This is in good agreement with Fig. 1(b), where mean values of the interlayer coupling constants J_1 and J_2, determined by fitting the VSM and MOKE hysteresis loops as indicated in Sec. II, are plotted as a function of the spacer thickness. For each Ru thickness, J_1 (J_2) presented here is the average between J_1 (J_2) obtained from VSM and that obtained from MOKE. Positive values of J_1 indicate FM coupling and negative values indicate AF coupling (when J_2 is neglected). One clearly recognizes an oscillatory behavior of J_1 as a function of the spacer thickness, which is attenuated for larger d_{Ru}. The coupling is purely FM and AF for

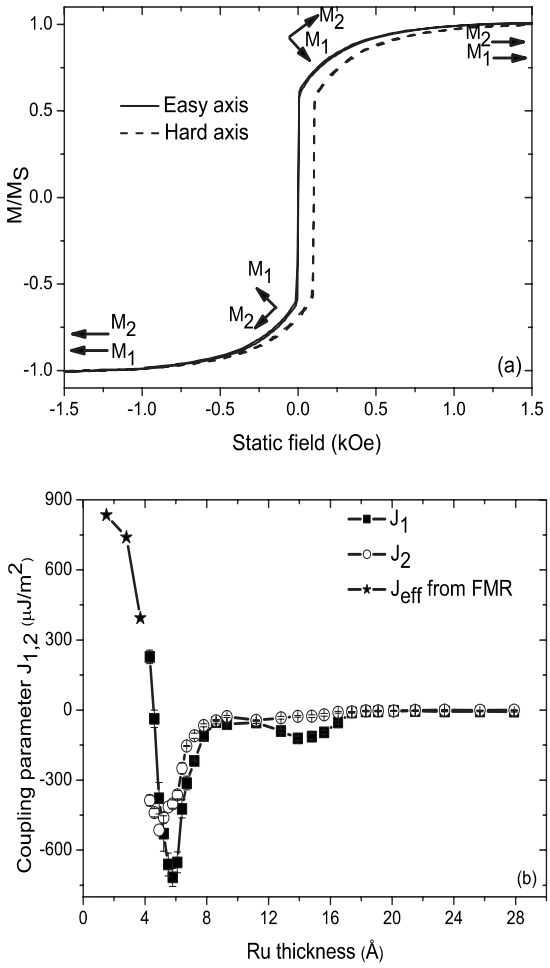

FIG. 1. (a) Easy and hard axis hysteresis loops of Si/Ta/NiFe(30 nm)/Ru(4.9 Å)/NiFe(30 nm)/Ta obtained by vibrating sample magnetometer (VSM). Arrows indicate the magnetization states for different applied fields. (b) Mean values of the bilinear (J_1) and biquadratic (J_2) interlayer coupling constants of Si/Ta/NiFe(30 nm)/Ru(d_{Ru})/NiFe(30 nm)/Ta as a function of the Ru thickness. The coupling constants have been determined by fitting the VSM and MOKE hysteresis loops numerically for antiferromagnetically coupled samples and by FMR for ferromagnetically coupled ones (effective coupling). For each Ru thickness, J_1 (J_2) presented here is the average between J_1 (J_2) obtained from VSM and that obtained from MOKE. The corresponding error bar for J_1 and J_2 is also given.

$d_{Ru}<4.3$ Å and $d_{Ru}>6.7$ Å, respectively, and a non-negligible biquadratic coupling is present for samples of Ru thicknesses between these two regimes. The oscillation period is 8.5 Å and slightly smaller than usually measured in the Co/Ru systems (about 11 Å).

B. Dynamic measurements by pulsed inductive microwave magnetometer and vector network analyzer ferromagnetic resonance

In analogy with coupled harmonic oscillators, the magnon modes in two magnetic films coupled via a nonmagnetic interlayer can be classified into acoustic and optic modes de-

pending on whether the two film magnetizations precess in phase or out of phase, respectively. This assignment is straightforward when the film magnetizations are in parallel alignment. For the antiparallel configuration, the two magnetizations precess in opposite directions, and hence, their relative phase changes continuously.

Behavior of the spin-wave frequencies as a function of applied fields provides a great deal of information about the magnitude and functional form of the coupling energy. Over the whole range of the spacer thickness, the typical experimental resonance frequencies as a function of the external in-plane bias field (H), measured by PIMM and VNA-FMR, are shown in Figs. 2(a) and 2(b) for two Ru thicknesses of 4.9 and 14.8 Å. For d_{Ru}=4.9 Å, both J_1 and J_2 are large and the AF coupling is strong, while for d_{Ru}=14.8 Å, the coupling is weak and mainly J_1 exists. Our experimental results have been fitted by the model presented in Ref. 10 using the parameters indicated in the caption of Fig. 2. These two samples show qualitatively similar behavior and will be discussed together. There are two different frequencies which appear in different field regimes. The variation of the mode frequencies with the external magnetic field relates to the different magnetic states of the two NiFe magnetizations. These modes are identified as the optic and acoustic spin-wave modes of the coupled ferromagnetic films. This has been confirmed by our simulations by comparing the phases of the two modes after numerical solution of the LLG equation. It is also in good agreement with the model of Zivieri *et al.*[9] which predicts that for AF coupled films and at low bias fields, the acoustic mode has the lower frequency while the optic mode has the higher frequency. However, above a critical applied field (H_{cr}), which is coupling dependent [see Fig. 2(c)] a crossover between the two mode frequencies occurs and the situation is reversed (i.e., the position of the acoustic mode frequency switches with that of the optic one), as indicated in Fig. 2. Thus, in AF coupled multilayers, the magnetic ground state develops as a function of the applied field and the classification of "acoustic" and "optic" modes as lower and higher frequency modes, respectively, is not generally valid. Therefore, the knowledge of the magnetization state corresponding to the applied bias field is necessary when identifying these modes.

We note that in order to resolve the optic mode over a large field range and, in particular, at its intersection with the acoustic mode, we used a different measurement configuration similar to the longitudinal FMR, which is more sensitive to the optical mode. Therefore, instead of applying the rf field perpendicular to the bias field, both fields were parallel to each other. We note that, in this case, both modes have a stronger signal in VNA-FMR compared to PIMM, where they can only be observed over a narrow field window (see Fig. 2).

Figure 2(b) shows that at very low fields ($0<H<20$ Oe) the magnetizations align antiparallel to each other [see inset of Fig. 2(b)]. Therefore, the optic mode has the higher frequency. The discontinuity in the frequencies seen in the simulations[10] at 20 Oe reflects the spin-flop transition. In this spin-flop phase ($H>20$ Oe), the angle between the magnetizations continuously decreases from 180° to 0°.

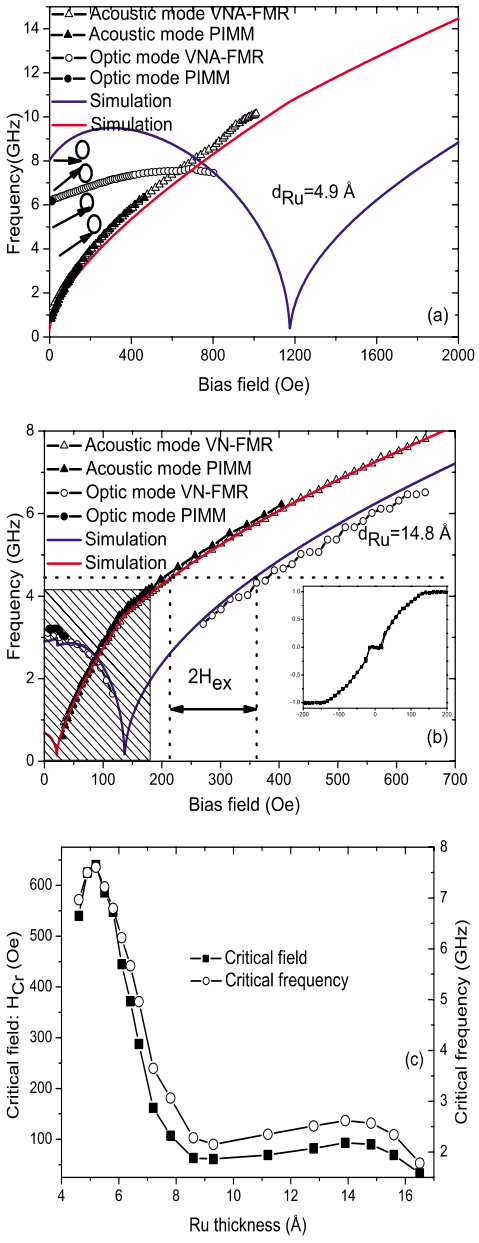

FIG. 2. (Color online) Frequencies of the optic and acoustic modes of Si/Ta/NiFe(30 nm)/Ru(d_{Ru})/NiFe(30 nm)/Ta structure as a function of the in-plane bias field and for (a) d_{Ru}=4.9 Å and (b) d_{Ru}=14.8 Å. These frequencies are obtained by fitting the module of the transmission coefficient S_{21} measured by VNA-FMR to a Lorentzian and by the Fourier transform of the time-domain magnetic response measured by PIMM. Pulse field of 8.5 Oe is used for PIMM measurements. The effective exchange field is given by the field difference above the saturation between the corresponding resonance fields at a fixed frequency, as indicated by the dotted lines. The inset shows the VSM easy axis hysteresis loop (normalized magnetization versus static field in Oe). The corresponding simulations are obtained from the model of Ref. 10 using a uniaxial anisotropy field H_{ani}=5 Oe with (a) J_1=−377 μJ/m^2 and J_2=−514 μJ/m^2, and (b) J_1=−140 μJ/m^2 and J_2=−15 μJ/m^2. (c) Ru thickness dependence of the critical field (H_{cr}), which is the value of the bias field where the frequencies of the optic and acoustic modes are equal (crossover). The corresponding frequency, called critical frequency, is also represented here as a function of d_{Ru}.

Above 20 Oe, the optic mode frequency and intensity start to decrease before disappearing [Fig. 2(b)]. It should have a dip when the sample saturates [see simulation[10] in Fig. 2(b)]. The acoustic mode frequency increases continuously and forms a kink around the saturation field. In the saturated state beyond 140 Oe, both acoustic and optic mode frequencies increase with the field. Therefore, at a fixed frequency, the field difference between the optic and acoustic modes is equal to the effective exchange field ($2H_{ex}$). The obtained value for effective coupling is in good agreement with that obtained from the fit of the VSM and MOKE measurements.

In Fig. 2(a), similar behaviors to Fig. 2(b) are found, with the difference that the optic frequency increases slowly until it reaches a maximum around 600 Oe, where again it starts to decrease. This behavior has also been reported by Kuanr *et al.* for Fe/Al/Fe trilayer.[16] We found this behavior for all the samples with 4.3 Å$\leqslant d_{\mathrm{Ru}} \leqslant$11.2 Å, where the estimated J_2 is larger than or comparable to J_1. The field, where the maximum of the optic mode frequency occurs, scales with the coupling strength. This behavior of the optic mode frequency reported in Fig. 2(a) is a consequence of the contribution of bilinear and biquadratic interlayer exchanges and Zeeman energy to the effective stiffness of the magnetizations and can be reproduced with a simple single spin model[10] using the mean values of J_1 and J_2 obtained from the fit of the VSM and the MOKE hysteresis loops [see Fig. 2(a) for simulations]. The frequency offset of the optic mode in the simulation is caused by the presence of a significant twisting of the magnetization along the film normal in the real sample. This additional effect can be treated by a multilayer simulation as shown by Buchmeier *et al.*[17]

The effect of the biquadratic coupling on the mode frequency has been studied theoretically by Layadi.[10] For antiferromagnetic coupling, two situations can arise. When the applied field is greater than the saturation field, the magnetizations are parallel and, for the same parameters, the resonant frequency of the acoustic mode is constant while that of the optic one decreases almost linearly as J_2 increases. On the other hand, and for the same parameters, when the magnetizations are antiparallel, the mode behavior is different. The resonant frequencies of the optic mode and the acoustic mode decrease as J_2 increases, and the amplitudes of both modes are nonzero and vary with J_2. Moreover, the effective coupling (J_{eff}) defined as $J_{eff}=J_1+2J_2$ and $J_{eff}=J_1-2J_2$ in the parallel and antiparallel states, respectively,[11] increases (decreases) with increasing J_2 ($J_2<0$) for antiferromagnetic coupling for parallel (antiparallel) states. Therefore, with increasing AF coupling strength, the optic mode frequency shifts up for antiparallel alignment and down for parallel alignment because the AF coupling represents a restoring force for the antiparallel alignment but not for the parallel alignment.[11]

For a fixed bias field value, the frequencies of the optic and acoustic modes oscillate as a function of d_{Ru} with the same period as J_1 (Fig. 3). The frequency of the optic mode strongly depends on the interaction, i.e., the interlayer coupling, whereas the acoustic modes (above saturation) are independent of the coupling strength, again in analogy to coupled harmonic oscillators. However, the acoustic mode frequency [Fig. 3(b)] depends on the alignment of the film

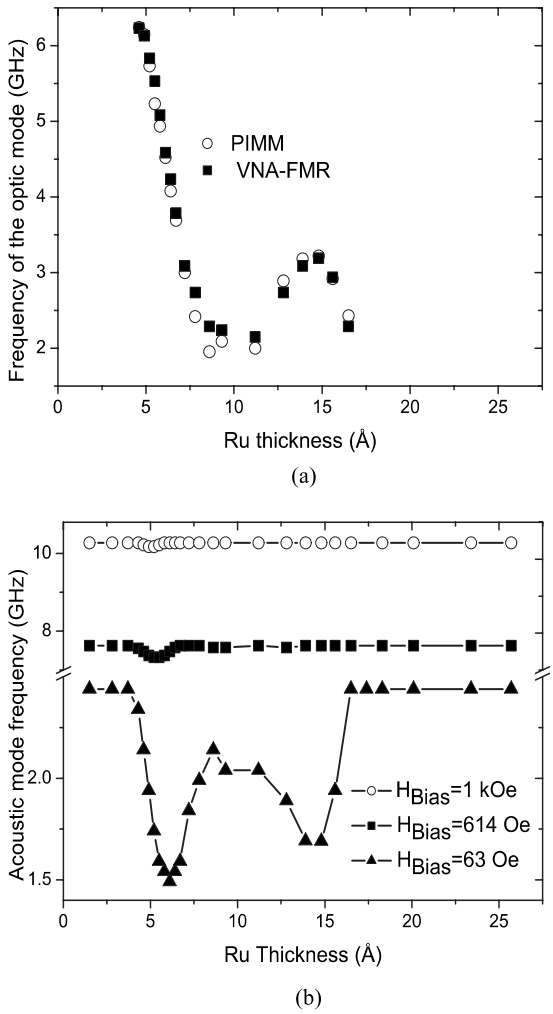

FIG. 3. Mode frequencies of the Si/Ta/NiFe(30 nm)/Ru(d_{Ru})/NiFe(30 nm)/Ta coupled system as a function of the spacer thickness d_{Ru}. (a) Optic mode frequencies measured by PIMM and VNA-FMR at an easy axis applied bias field of 5 Oe and (b) acoustic mode frequencies at the indicated easy axis applied bias fields. The acoustic mode frequencies presented here are obtained from VNA-FMR measurements.

magnetizations. This frequency is constant for strong FM coupled ($d_{\mathrm{Ru}} \leqslant$3.7 Å) and uncoupled NiFe ($d_{\mathrm{Ru}} \geqslant$16.5 Å) layers, where the two magnetizations are collinear and parallel to the applied field. Therefore, we attribute these oscillations of the acoustic mode as a function of d_{Ru}, which vanish [Fig. 3(b)] when the bias field is above 1 kOe (field where all the samples are mostly saturated), to the canting angle of the two magnetizations which is coupling dependent. Similar trends have been reported in Ref. 18.

C. Dynamic measurements by conventional ferromagnetic resonance

The typical obtained FMR spectrum at 22 GHz is shown in Fig. 4 for FM (d_{Ru}=3.7 Å), AF coupled (d_{Ru}=4.9 Å and d_{Ru}=14.8 Å), and uncoupled layers (d_{Ru}=18.3 Å). The two higher field modes (modes 3 and 4 in Fig. 4) are the usual acoustic and optic modes, while the two other modes at

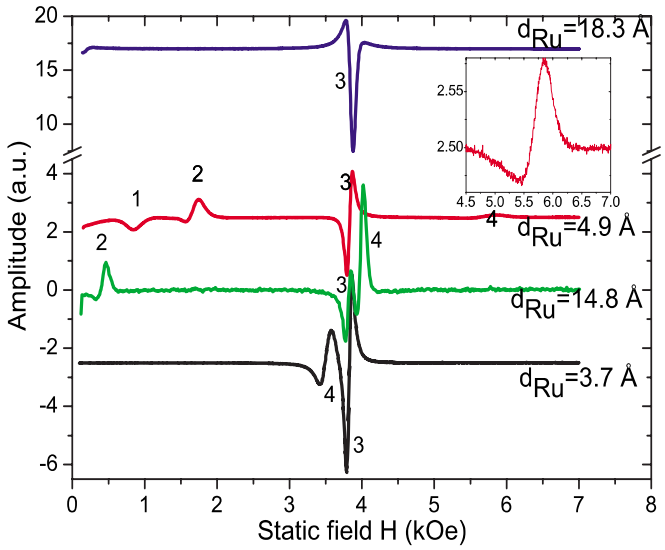

FIG. 4. (Color online) FMR spectrum of Si/Ta/NiFe(30 nm)/Ru(d_{Ru})/NiFe(30 nm)/Ta measured at 22 GHz. FMR signal is proportional to the field derivative of the imaginary part of the rf susceptibility. Each derivative is a mode and is referenced by an integer number to identify [(1) and (2)] the perpendicular standing spin waves (PSSW) corresponding to each NiFe layer, (3) the acoustic mode, and (4) the optic mode. The spectra have been shifted vertically with respect to that corresponding to d_{Ru}=14.8 Å for clarity. Inset shows a zoom in on the optic mode corresponding to d_{Ru}=4.9 Å.

lower fields (modes 1 and 2 in Fig. 4), which are observable at this frequency only for strong AF coupling (4.6 Å$\leqslant d_{Ru} \leqslant$6.4 Å), are supposed to be the first perpendicular standing spin wave (PSSW) corresponding to the two NiFe layers. The acoustic mode (mode 3 in Fig. 4) is independent of the exchange energy and, therefore, is degenerate with the resonance field of uncoupled system (Fig. 4). In the case of AF (FM) coupling, the optic mode is at higher (lower) field with respect to the acoustic mode. With increasing coupling, its resonance field increases (decreases).

In the case of thin film layer of thickness d_m, assuming long in-plane wavelengths and under the approximation of unpinned spins at the film surfaces which is well justified for NiFe due to the small anisotropies, the frequencies of the PSSWs are given by[19]

$$f_P = \frac{\mu_0 \gamma}{2\pi}\left(\left[H + \frac{2A}{M_{eff}}\left(\frac{P\pi}{d_m}\right)^2\right]\left[H + \frac{2A}{M_{eff}}\left(\frac{P\pi}{d_m}\right)^2 + M_{eff}\right]\right)^{1/2}, \quad (8)$$

where A is the exchange stiffness constant, H is the external magnetic field, γ is the gyromagnetic factor ($\gamma/2\pi$ =29.5 GHz/T for Permalloy), and P is the index of the PSSW mode.

The three lowest modes corresponding to P=0, 1, and 2 are represented in Fig. 5 for a NiFe layer of 30 nm in thickness for $\mu_0 M_{eff}$=1.064 T and $A=1.3\times10^{-11}$J/m.[20] Therefore, in our finite-band PIMM and VNA-FMR setups, we cannot observe PSSW modes ($P\geqslant1$). The FMR measurements at 22 and 35 GHz show that as the AF coupling

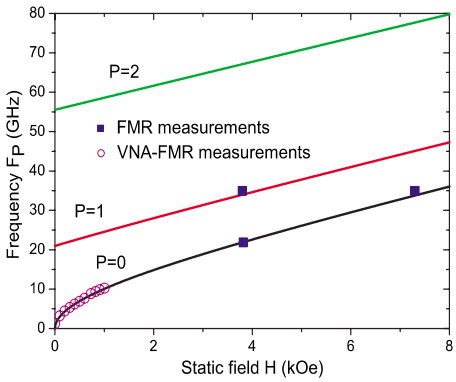

FIG. 5. (Color online) PSSW: P=1 and P=2, and uniform (acoustic) mode: P=0 corresponding to a NiFe thin film of 30 nm thickness obtained from Eq. (8) using $\mu_0 M_{eff}$=1.064 T, $A=1.3\times10^{-11}$ J/m, and $\gamma/2\pi$=29.5 GHz/T. Blue squares and cyan circles indicate respectively the corresponding FMR and VNA-FMR measurements of uniform mode (acoustic mode): P=0 and the first PSSW: P=1 for uncoupled layers [Si/Ta/NiFe(30 nm)/Ru(1.83 nm)/NiFe(30 nm)/Ta].

strength decreases, the resonance field of the PSSW moves to lower values in the same manner as the optic mode and in good agreement with the theoretical models.[21] Moreover, the effect of the interlayer coupling on the PSSW can be analyzed through the simple model proposed by Wigen *et al.*[22] This model assumes that each magnetic sublayer is resonating with a nearly uniform amplitude but different phase, caused by interlayer coupling via the spacer. In other words, different sublayers resonate at different amplitudes to give rise to an overall spin wave. This model can only be applied in the case that the interlayer coupling is much smaller than the intralayer one (the exchange coupling A should be divided by the lattice parameter to be compared to the interlayer coupling). Therefore, it is an extension of the spin-wave model for single layer magnetic thin films expressed by Eq. (8), and the exchange stiffness constant A can also be replaced by an effective coupling constant A_{eff}. Using this model, we calculated A_{eff} corresponding to the measured resonance fields of the PSSW modes at 22 GHz [Fig. 6(a)]. This plot shows clearly that AF interlayer coupling reduces the stiffness constant A_{eff}, and we converge to that of a single layer in the case of zero coupling. A_{eff} oscillates with the Ru thickness in the same manner as the interlayer coupling.

The PSSWs (P=1) were also observed at microwave frequency of 35 GHz, but their amplitudes were smaller compared to those observed at 22 GHz due to the low signal-to-noise ratio at this frequency. Therefore, in contrast to the measurements at 22 GHz, we observed only one PSSW (similar to mode 2 in Fig. 4). One should mention that in contrast to mode 2 (Fig. 4), the resonance fields of mode 1 at 22 GHz (observed for 4.6 Å$\leqslant d_{Ru} \leqslant$6.4 Å) are below the saturation fields in this Ru thickness range, suggesting that this mode (mode 1) is due to the canted magnetizations. Moreover, the PSSWs were not observed for the FM coupled sample ($d_{Ru}<4$ Å). The excellent agreement between FMR results obtained at 22 and 35 GHz for uncoupled layers and those calculated using Eq. (8) suggests that, as expected, the uniform (acoustic) mode is well fitted by this model (P=0)

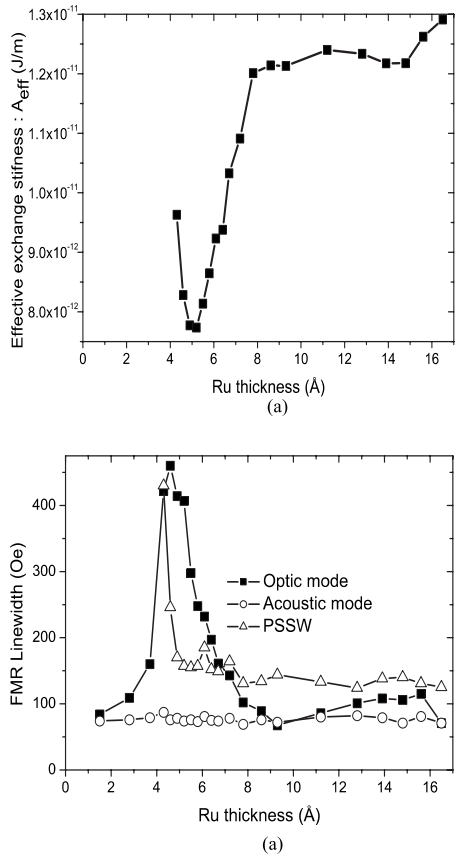

FIG. 6. Dependence of (a) the effective exchange stiffness coupling (A_{eff}) and (b) the FMR linewidth of the PSSW and the optic and acoustic modes on the spacer thickness d_{Ru} in Si/Ta/NiFe(30 nm)/Ru(d_{Ru})/NiFe(30 nm)/Ta coupled systems. The measurements presented here were carried out at 22 GHz. A_{eff} was calculated by replacing A by A_{eff} in Eq. (7) and using the measured PSSW resonance fields.

and confirms that the lower field peaks (mode 2) are the first PSSW modes.

Figure 6(b) shows the dependence of the FMR linewidth of optic, acoustic, and PSSW modes on the spacer thickness for the NiFe/Ru/NiFe trilayers. These linewidths represented here for FMR measurements at 22 GHz are defined as the peak-to-peak linewidths of the derivative Lorentzian. The key observation in Fig. 6(b) is that the linewidths of the acoustic and optic modes behave significantly differently. Like its resonance field, the linewidth of the acoustic mode is almost constant as a function of d_{Ru}. Assuming a linear dependence of the FMR linewidth (ΔH) on the microwave frequency (f) and fitting the measured results at 22 and 35 GHz to Eq. (9),[23] we have determined the effective Gilbert damping α as a function of Ru thickness d_{Ru}. The obtained results show that the damping is almost constant and fluctuate around an average damping of α=0.0073, which is in good agreement with NiFe thin films[24] (0.008 in Ref. 24). This can be explained by the fact that the magnetization vector of each FM layer is saturated at the resonance and the acoustic mode is independent of the exchange energy and, thus, is degenerate with the resonance mode of uncoupled system. Therefore, the fluctuation of α with d_{Ru} is due to the variations of the interface quality and to the inhomogeneities. This is also in agreement with the theoretical models which predict a constant linewidth in symmetrical coupled trilayers,[25]

$$\Delta H(f) = \Delta H(0) + 1.16\alpha\frac{2\pi f}{\gamma}, \tag{9}$$

where $\Delta H(0)$ is the zero-frequency offset and is caused by magnetic inhomogeneities and, therefore, its origin is extrinsic.

Due to the inhomogeneity of the exchange coupling, the linewidth of the optic mode is usually larger than that of the acoustic mode. Interestingly, the linewidth and the resonance field of the optic mode oscillate as function of d_{Ru} in the same manner as the coupling [see Figs. 1(b) and 6(b)]. This correlation with the coupling oscillations supports the explanation that the broadening of the linewidth is due to the inhomogeneous exchange interlayer coupling. However, in contrast to its resonance field, the linewidth of the PSSW does not oscillate with the Ru thickness d_{Ru}. Its decrease with d_{Ru} is drastically for small thickness, but it remains higher than that of the acoustic mode and the uncoupled layers. Moreover, this linewidth increases with the microwave frequency.

V. EFFECT OF THE PULSE FIELD AMPLITUDES

In our PIMM setup, we are able to increase the exciting pulse fields up to 150 Oe by applying voltage pulses of up to 200 V and 250 ps duration to the coplanar waveguide. Therefore, large excitation angles in both layers can be obtained. However, at such large precession angles, the frequency spectrum gets rather complex, and micromagnetic or at least macrospin (like in our case) simulations are helpful for interpreting the obtained results.

To validate our macrospin model presented in Sec. II, let us consider the case of the sample of 14.8 Å studied above in detail [Fig. 2(b)]. With increasing pulse fields, the PIMM measurements (Fig. 7) show two significant effects. First, it can be seen that the optic mode is observable over a larger range of the bias field, while the threshold (the bias field value where its intensity becomes significant) of the acoustic mode increases with higher pulse fields. Second, we observe at bias fields values around 100 Oe a higher harmonic of the acoustic mode. This behavior is well reproduced by the macrospin simulation (Fig. 7) despite the fact that the agreement decreases at the highest excitations (not shown here). This is an indication that at such high excitations, the macrospin approximation is no longer valid due to inhomogeneous precession.

For the sample with 6.4 Å of thickness and in addition to the optic and acoustic modes, we observe a very intense third mode for which the frequency varies strongly with the pulse field amplitude (Fig. 8). This mode, only observable in antiparallel configuration at low bias fields, has been observed for Ru thickness 6.1 Å$\leqslant d_{\text{Ru}} \leqslant$6.7 Å. As shown in Fig. 8, for low excitation amplitudes, only the optical mode is visible. With increasing pulse field amplitudes, a third mode appears and the acoustical mode becomes more intense. For higher excitation amplitudes, plenty of modes are present and only

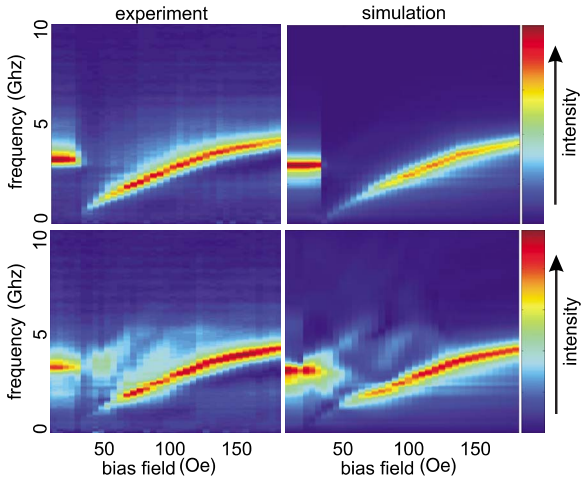

FIG. 7. (Color online) Comparison of PIMM results and macrospin simulations corresponding to optic and acoustic mode frequencies of Si/Ta/NiFe(30 nm)/Ru(14.8 Å)/NiFe(30 nm)/Ta for 8.5 Oe pulse field (upper row) and 85 Oe pulse field (lower row). The color scale indicates the mode intensities. The part of the graph represented here is hatched in Fig. 2(b).

the optic mode can be identified clearly. The pulse field dependence of this third mode frequency is most probably attributed to the large change of the direction of $\boldsymbol{H}_{J_1,i}$ and of the strength and direction of $\boldsymbol{H}_{J_2,i}$ as the magnetizations of the two layers undergo large excitation angles during the first nanosecond of the precession [compare Eq. (7)]. By this, the direction and also the strength of the effective field vary strongly in this time range. This is confirmed by the fact that this third mode is not visible any more in the fast Fourier transform spectrum when omitting the first 1.5 ns of the time-domain data, whereas the optic mode remains visible. However, this mode could not be reproduced by the macrospin simulation, suggesting that its origin lies beyond the macrospin model.

VI. CONCLUSION

The high frequency magnetization dynamics of interlayer coupled NiFe/Ru/NiFe films has been studied by three different methods. We detected two modes that we identified as optic and acoustic modes. The high frequency optic mode is dominant at low bias, while in higher fields, the acoustic mode has the largest intensity. The oscillatory nature of the

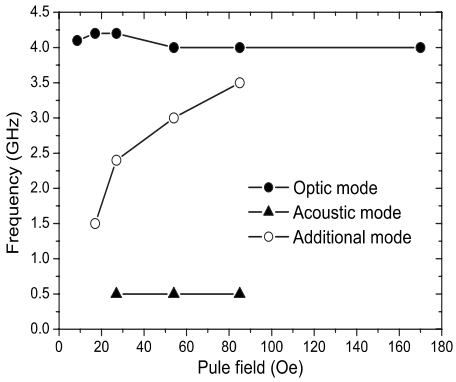

FIG. 8. Different mode frequencies for a Si/Ta/NiFe(30 nm)/Ru(6.4 Å)/NiFe(30 nm)/Ta sample at 8 Oe bias field where the magnetizations are in antiparallel configuration.

acoustic mode frequency, at low bias fields, with Ru thickness was attributed to the canting angle of the magnetizations. Comparison between PIMM and VNA-FMR in terms of frequency of modes shows good agreement, but the optic mode is more observable with VNA-FMR. The first mode of the perpendicular standing spin-waves has been observed with FMR for AF and uncoupled layers. The analysis of the obtained results via a simple model shows that the AF interlayer coupling reduces the effective exchange stiffness. Moreover, the FMR measurements showed different behaviors of the linewidths as a function of the spacer thickness for the optic and acoustic modes. The FMR linewidth of the different modes increases with the microwave frequencies, and typical damping constants of 0.0073 have been measured. The effect of the pulse field amplitudes on the properties of the different excited spin waves shows the existence of additional modes at high pulse field amplitudes for some samples. The macrospin simulations are in good agreement with the measurements.

ACKNOWLEDGMENTS

This work was supported in part by the European community's Marie Curie actions (Research Training Networks) under Contract No. MRTN-CT-2003-504462 and by Deutsche Forschungsgemeinschaft (DFG) SPP1133. The authors would like to thank C. Back for discussions and for putting at their disposal some experimental setups during this study, and M. Scheinfein for fruitful discussions regarding the macrospin simulations.

[1] P. Grünberg, R. Schreiber, Y. Pang, M. B. Brodsky, and H. Sowers, Phys. Rev. Lett. **57**, 2442 (1986).
[2] C. F. Majkrzak, J. W. Cable, J. Kwo, M. Hong, D. B. McWhan, Y. Yafet, J. V. Waszczak, and C. Vettier, Phys. Rev. Lett. **56**, 2700 (1986).
[3] M. B. Salamon, S. Sinha, J. J. Rhyne, J. E. Cunningham, R. W. Erwin, J. Borchers, and C. P. Flynn, Phys. Rev. Lett. **56**, 259 (1986).
[4] P. Grünberg, Acta Mater. **48**, 239 (2000).
[5] M. N. Baibich, J. M. Broto, A. Fert, F. Nguyen Van Dau, F. Petroff, P. Etienne, G. Creuzet, A. Friederich, and J. Chazelas, Phys. Rev. Lett. **61**, 2472 (1988).
[6] G. Binasch, P. Grünberg, F. Saurenbach, and W. Zinn, Phys. Rev. B **39**, 4828 (1989).
[7] B. N. Engel, J. Åkerman, B. Butcher, R. W. Dave, M. DeHerrera, M. Durlam, G. Grynkewich, J. Janesky, S. V. Pietambaram, N.

D. Rizzo, J. M. Slaughter, K. Smith, J. J. Sun, and S. Tehrani, IEEE Trans. Magn. **41**, 132 (2005).
[8] C. H. Back, R. Allenspach, W. Weber, S. S. P. Parkin, D. Weller, E. L. Garwin, and H. C. Siegmann, Science **285**, 864 (1999).
[9] R. Zivieri, L. Giovannini, and F. Nizzoli, Phys. Rev. B **62**, 14950 (2000).
[10] A. Layadi, Phys. Rev. B **65**, 104422 (2000).
[11] B. K. Kuanr, M. Buchmeier, R. R. Gareev, D. E. Bürgler, R. Schreiber, and P. Grünberg, J. Appl. Phys. **93**, 3427 (2003).
[12] L. C. C. M. Nagamine, J. Geshev, T. Menegotto, A. A. R. Fernandes, A. Biondo, and E. B. Saitovitch, J. Magn. Magn. Mater. **288**, 205 (2005).
[13] L. Landau and E. Lifshitz, Phys. Z. Sowjetunion **8**, 153 (1935); T. L. Gilbert, Phys. Rev. **100**, 1243 (1955).
[14] T. Martin, B. Becker, S. Ganzer, T. Hagler, M. Sperl, and G. Bayreuther, J. Appl. Phys. **97**, 10A718 (2005).
[15] I. Neudecker, G. Woltersdorf, B. Heinrich, T. Okuno, G. Gubbiotti, and C. H. Back, J. Magn. Magn. Mater. **307**, 148 (2006).
[16] B. K. Kuanr, M. Buchmeier, Daniel E. Bürgler, and P. Grünberg, J. Appl. Phys. **91**, 7209 (2002).
[17] M. Buchmeier, B. K. Kuanr, R. R. Gareev, D. E. Bürgler, and P. Grünberg, Phys. Rev. B **67**, 184404 (2003).
[18] J. Fassbender, F. Nörtemann, R. L. Stamps, R. E. Camley, B. Hillebrands, G. Güntherodt, and S. S. P. Parkin, Phys. Rev. B **46**, 5810 (1992).
[19] S. O. Demokritov and B. Hillebrands, in *Spin Dynamics in Confined Magnetic Structures I*, edited by B. Hillebrands and K. Ounadjela (Springer, Berlin, 2002), p. 70.
[20] R. P. van Gorkom, J. Caro, S. J. C. H. Theeuwen, K. P. Wellock, N. N. Gribov, and S. Radelaar, Appl. Phys. Lett. **74**, 422 (1998).
[21] B. Hillebrands, Phys. Rev. B **41**, 530 (1990).
[22] P. E. Wigen, Z. Zhang, S. Iwata, and T. Suzuki, J. Magn. Soc. Jpn. **15**, 33 (1991).
[23] B. Heinrich, J. F. Cochran, and R. Hasegawa, J. Appl. Phys. **57**, 3690 (1985).
[24] W. K. Hiebert, A. Stankiewicz, and M. R. Freeman, Phys. Rev. Lett. **79**, 1134 (1997).
[25] A. Layadi and J. O. Artman, J. Magn. Magn. Mater. **92**, 143 (1990).